Impedance-based Stability Analysis for HVDC Diode-Rectifier Connected Off-shore Wind Farms

S. Añó-Villalba, S. Bernal-Perez, J. Martinez-Turegano, R. Blasco-Gimenez
Universitat Politècnica de València, Spain
sanyo@die.upv.es, sbernal@die.upv.es, jaumartu@upv.es, r.blasco@ieee.org

***Abstract*—This paper includes a stability study of a HVDC diode rectifier connected off-shore wind power plant. Usually, the internal control strategy of commercial wind turbines are not completely known, so stability studies based on transfer functions or eigenvalue analysis are of limited use. However, the frequency behaviour of both wind turbine grid side converters and HVDC diode rectifier station can be obtained without a detailed knowledge of the control internals of the wind turbines.**

This paper includes the validation of impedance-based stability analysis for HVDC diode-rectfier connected off-shore wind farms. The frequency dependent impedance of the wind turbine converters and of the diode rectifier HVDC station are developed both analytically from their respective analytical models and also by using signal injection.

It is shown that the stability analysis using the identified impedance frequency response and that from analytic calculation lead the same results, thus validating the use of the impedance method for the stability analysis of grid-forming Diode-rectifier connected wind power plants.

***Index Terms*—HVdc transmission control, Wind power generation, Voltage stability, Impedance estimation, Generalysed Nyquist Analysis.**

I. Introduction

The connection of generation units to HVDC links using diode rectifiers has been proposed as a robust an efficient method for uni-directional transmission of generated power [1]–[3]. The direct connection of synchronous generators to HVDC diode rectifier stations present important technical disadvantages, as the relatively large delays on synchronous generator voltage control lead to very poor short-circuit performance [3].

However, these control limitations can be overcome with the use of wind turbines using fully rated converters. With this kind of wind turbines, it is possible to control the HVDC diode rectifier stations to provide good regulation and excellent fault performance [4]–[8]. Moreover, it is claimed that the use of HVDC diode rectifier stations can lead to up to 30% saving on large wind power plant transmission costs [9], [10].

There are several techniques for the control of a HVDC diode-rectifier connected wind power plant, all of them based on grid-forming converters. The stability analysis of such connections is paramount to ensure adequate performance in the complete operational range [11]. However, the internal control strategy of the wind turbine converters is generally not made available by the wind turbine manufacturers.

Alternatively, stability studies based on harmonic impedance analysis can be used to analyze the small-signal behavior of the wind turbine converters without a direct knowledge of the wind turbine control internals [12]–[14].

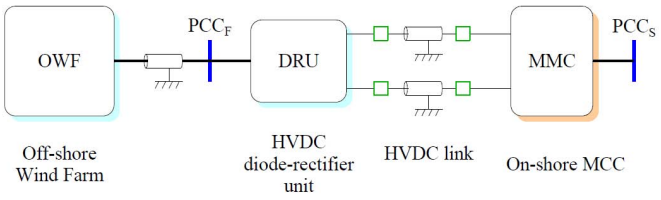

Fig. 1. Off-shore wind farm connected to the on-shore MMC through a diode based HVDC rectifier station.

The main aim of this paper is to present and validate a procedure for the harmonic impedance stability analysis of electrical systems including grid-forming wind turbine generators (WTG) and Diode Rectifier Units (DRU).

In order to ensure the validity of the proposed impedance based stability method, the state space model fo the complete system has been developed [15]. The harmonic impedance is obtained from both the analytical and the PSCAD models [13], in the latter case by means of disturbance injection. Finally, it is shown that the conclusions regarding system stability are the same using: a) the state space model, b) the impedance based model, c) the PSCAD detailed simulation.

Therefore, this paper shows the validity of the harmonic impedance stability method to predict system oscillations in DRU connected wind farm.

II. Impedance Based Stability Analysis

The system proposed is shown in fig. 1. The wind power plant (WPP) is modeled considering an aggregated equivalent of 50 8MW full converter WTGs. The impedance based stability analysis is carried out considering the frequency dependent impedance looking at both sides of PCC_F.

The system is split between the source and the load subsystems, as in [13]. Figure 2 shows the location of the interfacing point between the source (WT) and the load (DRU). The source consists of WT ac-grid converter, LC-filter and transformer, while the load consists of ac-Cable, and DRU ac-filter, transformers, diode bridges and dc-filter.

To validate the accuracy of the analytical study, a PSCAD frequency scan is numerically performed. This frequency scan is obtained by applying a small current disturbance at a certain frequency to the WPP current. The PCC voltage is measured,

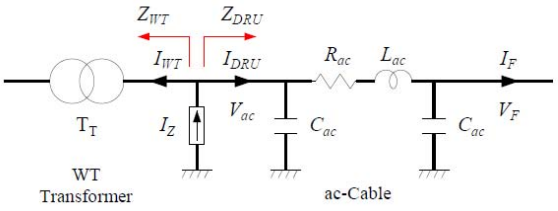

Fig. 2. Injection of a small disturbance I_Z to compute WT and DRU impedances.

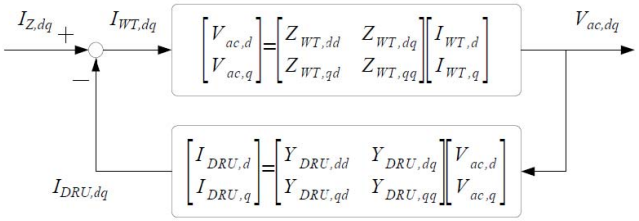

Fig. 3. Z_{WT} and Z_{DRU} relationship.

and the harmonic components of the disturbance frequency are obtained.

The source or WT impedance ZWT can be calculated from the input-output relation as:

$$V_{ac} = Z_{WT} I_{WT} \tag{1}$$

Similarly, the load or DRU impedance ZDRU can be calculated as:

$$V_{ac} = Z_{DRU} I_{DRU} \tag{2}$$

The impedance based analysis is carried out in a rotating d-q axis.The WTG dq-impedance will be:

$$\begin{pmatrix} V_{ac,d} \\ V_{ac,q} \end{pmatrix} = \begin{pmatrix} Z_{WT,dd} & Z_{WT,dq} \\ Z_{WT,qd} & Z_{WT,qq} \end{pmatrix} \begin{pmatrix} I_{ac,d} \\ I_{ac,q} \end{pmatrix} \tag{3}$$

and the DRU dq-impedance is:

$$\begin{pmatrix} V_{ac,d} \\ V_{ac,q} \end{pmatrix} = \begin{pmatrix} Z_{DRU,dd} & Z_{DRU,dq} \\ Z_{DRU,qd} & Z_{DRU,qq} \end{pmatrix} \begin{pmatrix} I_{DRU,d} \\ I_{DRU,q} \end{pmatrix} \tag{4}$$

Therefore, both Z_{WT} and Z_{DRU} can be obtained from both the state-space equations and by disturbance injection at the point shown in fig. 2.

The small-signal stability of the system can then be assessed by the impedance-based approach through the frequency domain Generalized Nyquist Criterion (GNC) [16], [17]. For this approach the system is split between the impedance of the source ($Z_{WT,dq}$) and the load ($Z_{DRU,dq}$) as shown in Figure 2.

At the interfacing point, voltages and currents can be represented by the block diagram shown in Figure 3. The corresponding closed-loop transfer function is:

$$V_{ac,dq} = \left(I + Z_{WT} Y_{DRU}\right)^{-1} Z_{WT} I_{Z,dq} \tag{5}$$

As Z_{WT} is designed to be stable, the stability of the system can be found by checking the generalized Nyquist criterion on the loop impedance $L_{dq} = Z_{WT} Y_{DRU}$.

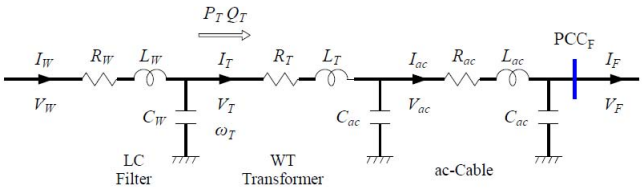

Fig. 4. WT filter, transformer and ac-cable.

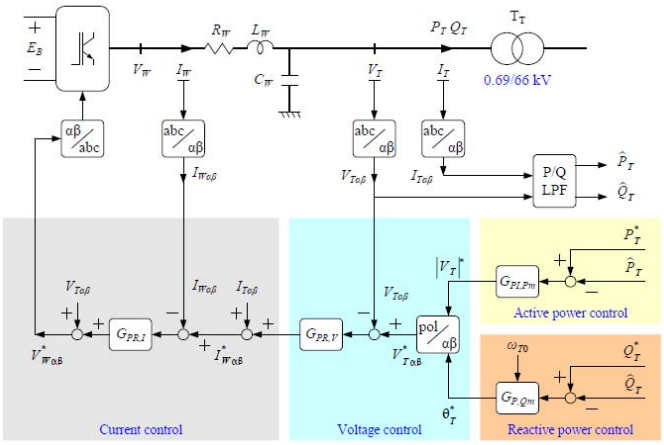

Fig. 5. Grid side converter control

III. Wind Turbine Control

The considered WPP consists of 50 WTGs arranged in 6 strings, and it is aggregated using system order reduction techniques which ensure a faithful representation of the array cable main resonant peak [18].

Figure 5 shows a typical control strategy for DRU-connected WTGs. The inner current and voltage loops are designed in a stationary ($\alpha - \beta$) frame using proportional-resonant (PR) controllers. As the system is DRU-connected and it is capacitive- dominated, the outer loop includes P-V and Q-ω droops.

Considering current control loops with PR controllers, $G_{PR,I}(s)$ is:

$$G_{PR,I}(s) = K_{PI} + K_{RI} \frac{s}{s^2 + \omega_{PR}^2} \tag{6}$$

Similarly, the outer voltage loops are also based on stationary frame PR controllers, which, for analysis purposes, will also be expressed in a synchronous d-q frame of reference. The transfer function of the voltage loop PR controllers is:

$$G_{PR,V}(s) = K_{PV} + K_{RV} \frac{s}{s^2 + \omega_{PR}^2} \tag{7}$$

The dynamics of the P and Q droops are developed as follows. Active and reactive power measurement are filtered

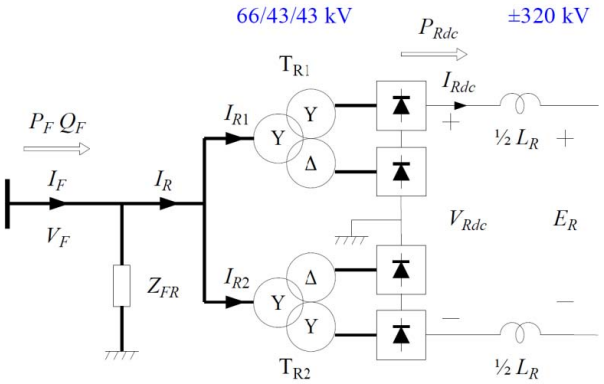

Fig. 6. Diode-based HVDC rectifier unit.

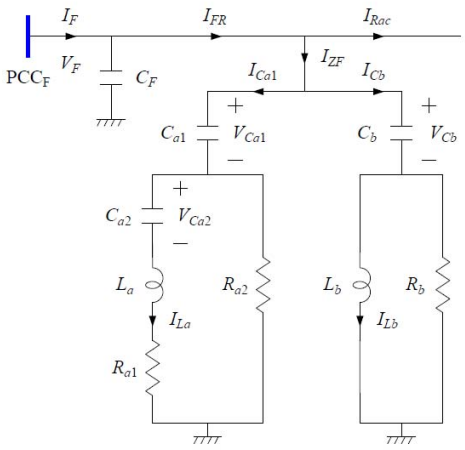

Fig. 7. DRU ac-filter Z_{FR}.

as per:

$$P_{TF}(s) = \frac{\omega_{PQ}}{s+\omega_{PQ}} P_T(s) \tag{8}$$

$$Q_{TF}(s) = \frac{\omega_{PQ}}{s+\omega_{PQ}} Q_T(s) \tag{9}$$

The active power control loop is:

$$|V_T|^* = K_{P,Pm}\left(P^*_{TF} - P_{TF}\right) + K_{I,Pm}\frac{1}{s}\left(P^*_{TF} - P_{TF}\right) \tag{10}$$

and the reactive power control loop is:

$$\theta^*_T = K_{P,Qm}\left(Q^*_{TF} - Q_{TF}\right) + \omega_{T0}t \tag{11}$$

The reference voltage V^*_T is expressed in the synchronous frame rotating at ω_{T0} as:

$$V^*_{Td} = |V_T|^* \cos\beta_T \tag{12}$$

$$V^*_{Tq} = |V_T|^* \sin\beta_T \tag{13}$$

where:

$$\beta_T = \theta^*_T - \omega_{T0}t = K_{P,Qm}\left(Q^*_{TF} - Q_{TF}\right) \tag{14}$$

The DRU model is shown in Figure 6, where Z_{FR} represents the ac-filter and capacitor banks shown in Figure 7.

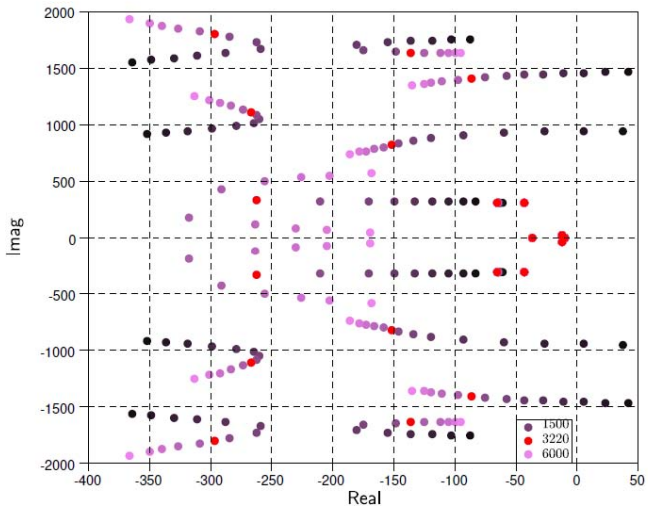

Fig. 8. Root locus of the system (WT and DRU) as a function of K_{PI} (zoom).

The DRU dynamic equations are expressed in a global dq-frame-F, which rotates at a frequency $\omega_F = \frac{d}{dt}\theta_F$. Note DRU dynamic equations are expressed in a synchronous frame of reference which is generally not the same as the one used for the derivation of WTG dynamics. The reason for this is that naturally, the equations for the diode rectifier are simpler if expressed in a frame of reference which is oriented to the diode rectifier ac-grid voltage (V_F in Figure 6).

IV. State-Space based Stability Analysis

As mentioned in the introduction, the state space model of the complete system is developed as a benchmark to validate the results of the impedance based stability analysis. The WTG state space model will include both the controls and the system physical elements.

Both state space model and harmonic impedance stability analysis are carried out in a synchronous rotating d-q frame as this is a more suitable choice for DRU modeling.

Fig. 8 shows the root locus of the system as a function of the current PR controller proportional gain (K_{PI}) when P^*_F = 0.5 pu and Q^*_F = 0 pu. The values of K_{PI} change from 1500 (dark) to 6000 (light). The system becomes unstable when K_{PI} decreases from 2100 to 1900.

V. Impedance-based Stability Analysis Results

A. Wind turbine impedances in dq-frame

This section compares the d-q frame WTG impedances obtained from the state space equations and those obtained from PSCAD by means of signal injection (Fig. 2). The considered operating point is defined by $P^*_T = 0.5$ pu and $Q^*_T = 0$ pu. Figs. 9 and 10 show the resulting WTG dq-impedances ($Z_{WT,dq}$).

To verify the theoretical analysis, a simulation has been carried out in PSCAD. The resulting dq-impedances are shown as circles in Figs. 9 and 10 and they closely match the analytical

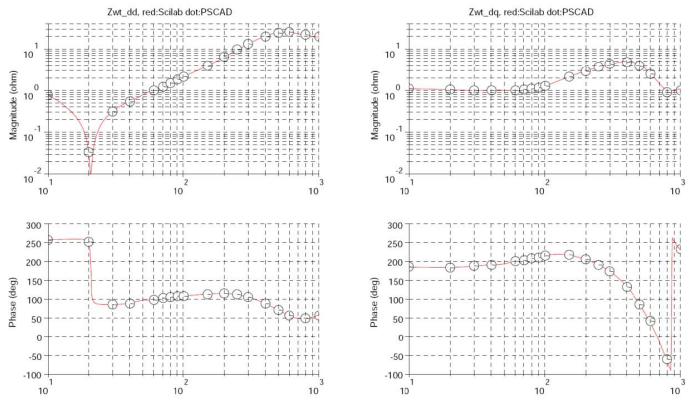

Fig. 9. $Z_{WT,dd}$ and $Z_{WT,dq}$ impedance of the wind turbine as a function of the frequency (Hz) ($K_{PI} = 3220$).

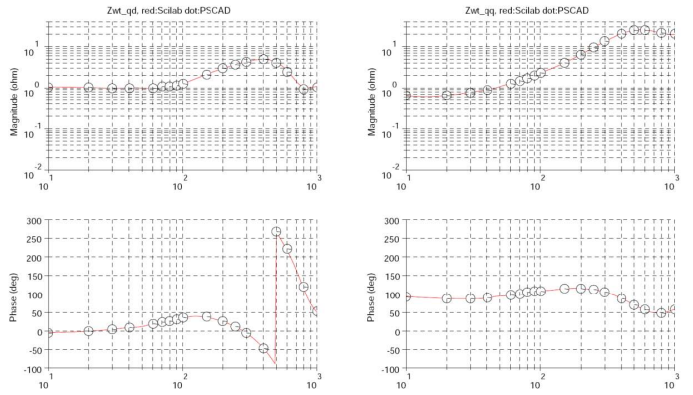

Fig. 10. $Z_{WT,qd}$ and $Z_{WT,qq}$ impedance of the wind turbine as a function of the frequency (Hz) ($K_{PI} = 3220$).

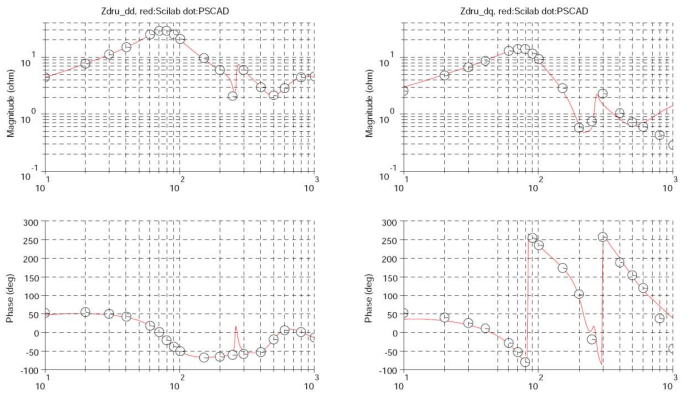

Fig. 11. $Z_{DRU,dd}$ and $Z_{DRU,dq}$ impedance as a function of the frequency (Hz).

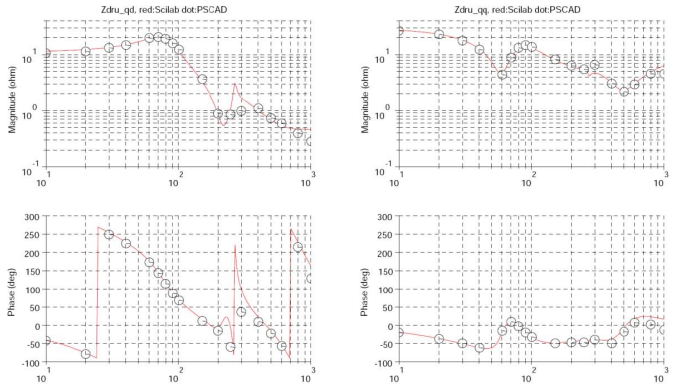

Fig. 12. $Z_{DRU,qd}$ and $Z_{DRU,qq}$ impedance as a function of the frequency (Hz).

results. Clearly, both PSCAD and state space WTG impedance calculations closely match each other, therefore validating the procedure carried out to obtain the WTG impedance.

B. DRU Impedance in dq-frame

The same procedure used for the calculation and validation of WTG d-q impedances is now applied to the DRU station (which includes capacitor and filter banks, diode rectifiers, transformers and dc smoothing reactor). The resulting DRU dq-impedances are shown in Figs. 11 and 12.

As in the previous case, the impedances obtained from PSCAD simulations show a very close match to the analytical calculation. The few existing discrepancies are at frequencies that correspond to the DRU switching harmonics.

As previously shown, the dq impedance matrices obtained from the analytical studies and those obtained from PSCAD identification of the detail system agree to a very large extent. Therefore, those impedances can be used in order to analyse the harmonic stability of the connected system.

Fig. 13 shows the loop impedance ($L_{dq} = Z_{WT}Y_{DRU}$) eigenvalues, both from the analytical model and from the PSCAD identified impedances for the baseline case ($K_{PI} = 3220$). Both results have an excellent degree of agreement up to 600Hz, as previously mentioned. At 600Hz the phase of one of the eigenvalues calculated from PSCAD is very different from that obtained from the analytical model. Reasons for this discrepancy are that the average value analytical DRU model does not consider the commutation harmonics which are present in the detailed PSCAD simulation.

Fig. 14 shows the eigenvalues of the loop transfer function $L_{dq} = Z_{WT}Y_{DRU}$ for different frequencies and for the value of the WTG current loop resonant controller proportional gain ($K_{PI} = 2100$).

Fig. 15 shows the same graph as the previous figure, but considering a reduced gain $K_{PI} = 1900$. Clearly, the generalised Nyquist diagram does not encircle the -1 point for K_{PI}=2100, whereas, when the K_{PI} gain is reduced to K_{PI}=1900, the -1 point is now encircled. Therefore, Fig. 15 shows that the system is now unstable.

Fig. 15 shows that the cross-over frequency of the eigenvalue causing instability is around 230Hz, since at this frequency, is where the eigenvalue magnitude is 0dB and its phase 180º.

This result is in clear agreement with results of the root-locus analysis carried out previously and with the detailed PSCAD EMT simulation results shown in Fig. 17, which both show an unstable 230 Hz oscillation when $K_{PI} = 1900$.

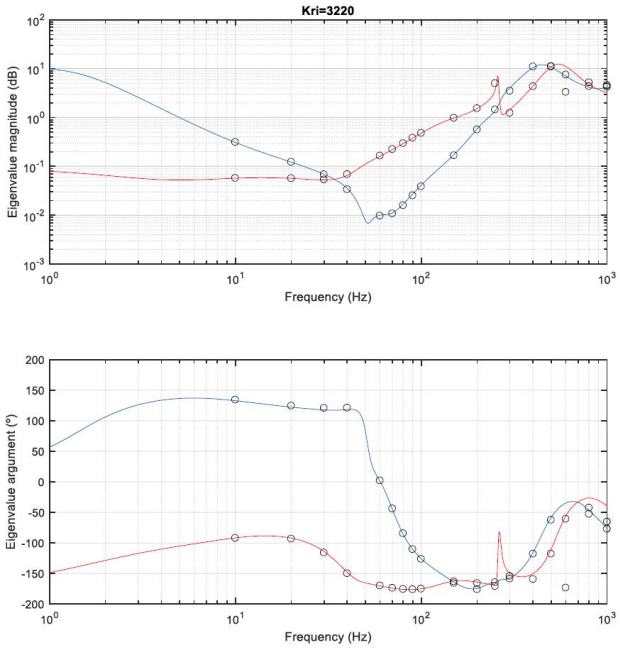

Fig. 13. Loop impedance matrix eigenvalues for $K_{PI} = 3220$.

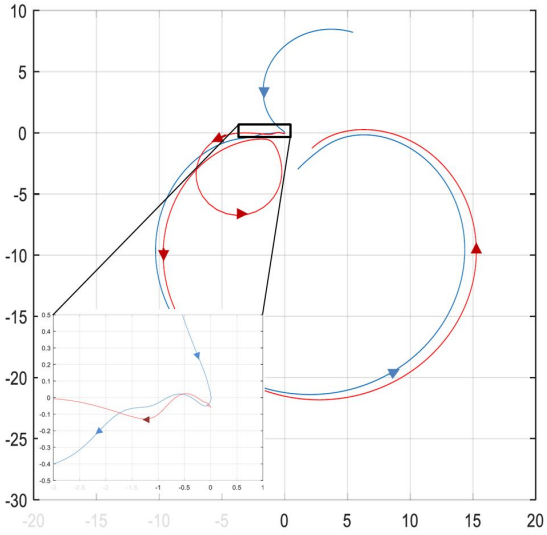

Fig. 14. Generalised Nyquist plot for $K_{PI} = 2100$.

VI. Discussion and Conclusions

As mentioned in the introduction, small-signal state space analysis has been used in order to validate both the harmonic impedance derived from PSCAD and the stability results obtained by means of the generalised Nyquist criterion.

Obviously, the state space representation allows for a more detailed model of the considered system and for its small-signal simulation. However, in many cases a state space representation is not practical, as a full model of the system and all the controllers would be required.

Therefore, the harmonic impedance of both grid-forming converter and DRU station have been obtained directly from

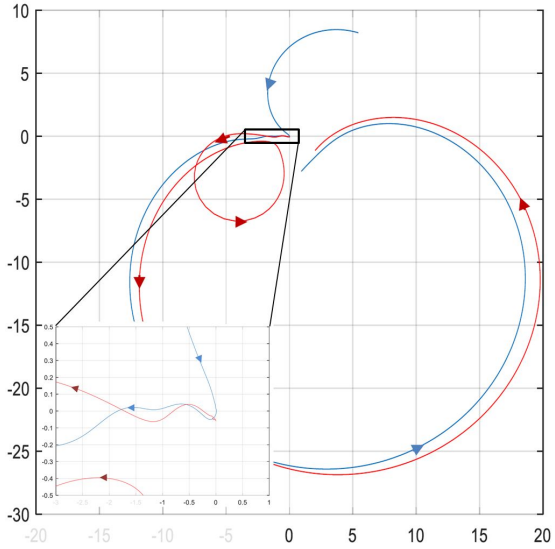

Fig. 15. Generalised Nyquist plot for $K_{PI} = 1900$.

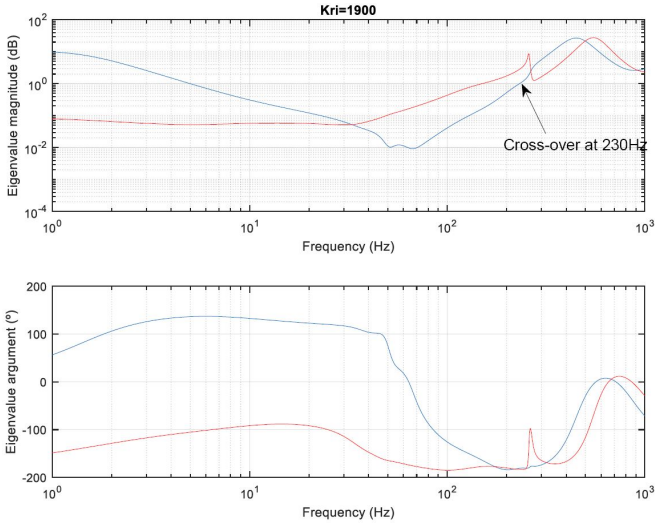

Fig. 16. Eigenvalues of loop transfer function $Z_{WT,dq}Y_{DRU,dq}$ as a function of frequency ($K_{PI} = 1900$).

the PSCAD model by means of perturbation injection.

As expected, both analytical and PSCAD-derived impedances show an excellent degree of agreement.

Based on the previous results, the generalized Nyquist diagrams have been obtained for two different values of the WTG current resonant controller proportional gain (K_{PI}), showing the transition between stability and instability. The results obtained by means of the generalised Nyquist criterion agree with those obtained from root-locus analysis, with the advantage that the impedance matrices used for the generalized Nyquist criterion can be obtained experimentally without needing to know the details of the WTG controllers.

The presented study has some limitations, including the limited usability of the generalized Nyquist criterion for WTG control design, as physical meaning of the closed loop eigen-

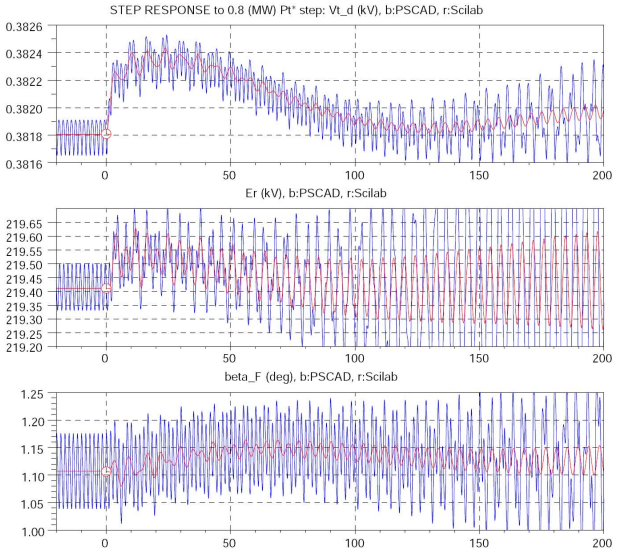

Fig. 17. PSCAD detailed simulation of the complete system showing unstable oscillations at 232Hz.

values is not, generally, straightforward.

In any case, this paper has shown that impedance based stability analysis is an adequate tool to predict harmonic oscillations in HVDC-DRU connected wind power plants.

Acknowledgements

The authors would like to thank the support of the Spanish Ministry of Science, Innovation and Universities and EU FEDER funds under grant DPI2017-84503-R. This project has received funding from the *European Union's Horizon 2020 research and innovation program* under grant agreement No. 691714.

VII. Appendix

Aggregated Wind Turbines		
Grid-side converter: 0.69 kVac, 50 Hz, 400 MW		
Transformer: T_{Wi}: 0.69/66 kV	$R_T = 0.004$ pu	$L_T = 0.1$ pu
LC-Filter: $R_W = 0.008$ pu	$X_W = 0.1$ pu	$C_W = 20pu$
HVdc Rectifier (based on Cigre benchmark model [19])		
Capacitor Bank: $C_F = 15.11\ \mu$F		
ZF-low frequency filter		
$C_{a1} = 48.24\ \mu$F	$C_{a2} = 536\ \mu$F	$L_a = 18.9$ mH
$R_{a1} = 4.12\ \Omega$	$R_{a2} = 36.29\ \Omega$	
ZF-high frequency filter		
$C_b = 48.24\ \mu$F	$R_b = 11.55\ \Omega$	$L_b = 1.88$ mH
Transformer $T_{R\Delta}$ and T_{RY}		
61/66 kV, 240 MVA	$X_{TR} = 0.18$ pu	
PR Controller Parameters		
Current Loop:	$K_{PI} = 3220$	$K_{RI} = 2.033 \times 10^6$
Voltage Loop:	$K_{PV} = 1477$	$K_{RV} = 2.262 \times 10^6$
Power Controller Parameters		
$K_{P,Pm} = 0.5478 \times 10^{-6}$	$K_{I,Pm} = 15.44 \times 10^{-6}$	$K_{P,Qm} = 0.7 \times 10^{-9}$

References

[1] T. Machida, I. Ishikawa, E. Okada, E. Karasawa, Control and protection of HVDC systems with diode valve converter, Electrical Engineering in Japan 98 (1) (1978) 62–70. doi:10.1002/eej.4390980109.
URL http://dx.doi.org/10.1002/eej.4390980109

[2] J. Bowles, Multiterminal HVDC transmission systems incorporating diode rectifier stations, Power Apparatus and Systems, IEEE Transactions on PAS-100 (4) (1981) 1674–1678. doi:10.1109/TPAS.1981.316562.

[3] S. Hungsasutra, R. M. Mathur, Unit connected generator with diode valve rectifier scheme, Power Engineering Review, IEEE 9 (5) (1989) 52–53. doi:10.1109/MPER.1989.4310694.

[4] S. Bernal-Perez, S. Añó-Villalba, R. Blasco-Gimenez, J. Rodríguez-D'Derleé, Efficiency and fault ride-through performance of a diode-rectifier- and VSC-inverter-based HVDC link for offshore wind farms, Industrial Electronics, IEEE Transactions on 60 (6) (2013) 2401–2409. doi:10.1109/TIE.2012.2222855.

[5] R. Blasco-Gimenez, N. Aparicio, S. Ano-Villalba, S. Bernal-Perez, LCC-HVDC Connection of Offshore Wind Farms With Reduced Filter Banks, IEEE Transactions on Industrial Electronics 60 (6) (2013) 2372 –2380. doi:10.1109/TIE.2012.2227906.

[6] S. Bernal-Perez, S. Ano-Villalba, R. Blasco-Gimenez, N. Aparicio, Connection of off-shore wind power plants to VSC-MTdc networks using HVdc diode-rectifiers, Industrial Electronics (ISIE), 2013 IEEE International Symposium on (2013) 1–6doi:10.1109/ISIE.2013.6563795.

[7] R. Blasco-Gimenez, S. Ano-Villalba, J. Rodriguez-D'Derlee, S. Bernal-Perez, F. Morant, Diode-Based HVdc Link for the Connection of Large Offshore Wind Farms, Energy Conversion, IEEE Transactions on (99) (2011) 1–12.

[8] R. Blasco-Gimenez, S. Añó-Villalba, J. Rodríguez-D'Derleé, F. Morant, S. Bernal-Perez, Distributed voltage and frequency control of off-shore wind farms connected with a diode-based HVdc link, Power Electronics, IEEE Transactions on 25 (12) (2010) 3095–3105. doi:10.1109/TPEL.2010.2086491.

[9] Peter Menke, New Grid Access Solutions for offshore wind farms, EWEA Off-shore 2015 (Mar. 2015).
URL http://www.ewea.org/offshore2015/conference/allposters/PO208.pdf

[10] Slavomir Seman, Rainer Zurowski, Timo Christ, Investigation of DC Converter Nonlinear Interaction with Offshore Wind Power Park System, EWEA Off-shore 2015 (Mar. 2015).
URL http://www.ewea.org/offshore2015/conference/allposters/PO214.pdf

[11] Soledad Bernal-Pérez, Integración híbrida multipunto en el sistema eléctrico de grandes parques eólicos marinos a través de redes de alta tensión en continua, Universitat Politècnica de València, Valencia, 2016.

[12] R. D. Middlebrook, S. Cuk, A general unified approach to modelling switching-converter power stages, in: 1976 IEEE Power Electronics Specialists Conference, 1976, pp. 18–34. doi:10.1109/PESC.1976.7072895.

[13] S. D. Sudhoff, S. F. Glover, P. T. Lamm, D. H. Schmucker, D. E. Delisle, Admittance space stability analysis of power electronic systems, IEEE Transactions on Aerospace and Electronic Systems 36 (3) (2000) 965–973. doi:10.1109/7.869516.

[14] M. Cespedes, J. Sun, Impedance Modeling and Analysis of Grid-Connected Voltage-Source Converters, IEEE Transactions on Power Electronics 29 (3) (2014) 1254–1261. doi:10.1109/TPEL.2013.2262473.

[15] S. Bernal-Perez, S. Ano-Villalba, R. Blasco-Gimenez, Stability analysis of HVDC-diode rectifier connected off-shore wind power plants, in: IECON 2015 - 41st Annual Conference of the IEEE Industrial Electronics Society, 2015, pp. 004040–004045. doi:10.1109/IECON.2015.7392729.

[16] J. F. BARMANJ, J. KATZENELSON§, A generalized Nyquist-type stability criterion for multivariable feedback systems, International Journal of Control 20 (4) (1974) 593–622. doi:10.1080/00207177408932763.
URL https://doi.org/10.1080/00207177408932763

[17] J. M. E. Valenca, C. J. Harris, A nyquist type criterion for the stability of multivariable linear systems, in: 1978 IEEE Conference on Decision and Control including the 17th Symposium on Adaptive Processes, 1978, pp. 821–823. doi:10.1109/CDC.1978.268041.

[18] J. Martínez-Turégano, S. Añó-Villalba, S. Bernal-Perez, R. Blasco-Gimenez, Aggregation of Type-4 Large Wind Farms Based on Admittance Model Order Reduction, Energies 12 (9) (2019) 1730. doi:10.3390/en12091730.
URL https://www.mdpi.com/1996-1073/12/9/1730

[19] M. Szechtman, T. Wess, C. V. Thio, First benchmark model for hvdc control studies, Electra (135) (1991) 54–73.